IEEE Access
Multidisciplinary ⋮ Rapid Review ⋮ Open Access Journal

Received 23 June 2023, accepted 15 August 2023, date of publication 22 August 2023, date of current version 30 August 2023.

Digital Object Identifier 10.1109/ACCESS.2023.3307637

RESEARCH ARTICLE

High-Reliability Non-Contact Photoplethysmography Imaging for Newborn Care by a Generative Artificial Intelligence

YENMING J. CHEN[1], LUNG-CHANG LIN[2], SHU-TING YANG[3], KAO-SHING HWANG[4,5], (Member, IEEE), CHIA-TE LIAO[6], AND WEN-HSIEN HO[5,7,8]

[1]Department of Information Management, National Kaohsiung University of Science and Technology, Kaohsiung 811, Taiwan
[2]Department of Pediatrics, Kaohsiung Medical University Hospital, Kaohsiung 807, Taiwan
[3]Division of Neonatology, Department of Pediatrics, Kaohsiung Medical University Hospital, Kaohsiung Medical University, Kaohsiung 807, Taiwan
[4]Department of Electrical Engineering, National Sun Yat-sen University, Kaohsiung 804, Taiwan
[5]Department of Healthcare Administration and Medical Informatics, Kaohsiung Medical University, Kaohsiung 807, Taiwan
[6]Division of Cardiovascular Medicine, Chi Mei Medical Center, School of Medicine, College of Medicine, National Sun Yat-sen University, Kaohsiung 804, Taiwan
[7]Department of Medical Research, Kaohsiung Medical University Hospital, Kaohsiung 807, Taiwan
[8]College of Professional Studies, National Pingtung University of Science and Technology, Pingtung City 912, Taiwan

Corresponding authors: Chia-Te Liao (drctliao@gmail.com) and Wen-Hsien Ho (whho@kmu.edu.tw)

This work was supported in part by the Chi-Mei Medical Center and Kaohsiung Medical University Research Foundation under Grant 110CM-KMU-06; in part by the Ministry of Science and Technology, Taiwan, under Grant MOST 111-2221-E-037-007 and Grant MOST 109-2410-H-992-018-MY2; and in part by the NSYSU-KMU Joint Research Project under Grant NSYSUKMU 112-P010.

This work involved human subjects or animals in its research. Approval of all ethical and experimental procedures and protocols was granted by the Institutional Review Board of Kaohsiung Medical University Hospital (KMUH) under Approval No. KMUHIRB-SV(I)-20210007.

ABSTRACT Long-term wiring on a newborn patient could be a disguise scene for parents. Unobtrusive and reliable monitoring without wiring can be a euphoric alternative for newborns and parents in obstetrics and gynecology (OB/GYN) incubation rooms. However, reliable and continuous non-contact surveillance in an incubation room is challenging. Therefore, a novel photoplethysmography imaging (PPGi) is developed specifically for baby skins through predictive adversarial adaptation and risk-sensitive generative synchronizer. Our artificial intelligence approach does not take blind guesses from input-output pairs. We apply an intelligent step to decouple the influence of fluctuated illumination through a generative algorithm of artificial intelligence. To boost skin detection performance, we capture those pixels with periodic variations and maximize the coherence of the extraction algorithm by the generative synchronizer. The periodic variations are matched by a synthesized pulse from the output PPGi signals through the control of a risk-sensitive filter to not over-compensate the illuminate variation. Based on the sensed pulsation, we synthesize the corresponding pulsation signals on the flight to identify the living skin in a spatiotemporal image sequence. We find that our skin classifier in risk-sensitive generative synchronizer effectively improves the quality of the resulting non-contact PPGi signal. Our algorithm produces substantial accuracy in the performance of PPGi reconstruction in the critical environment of newborn care. In the limited illustration of the incubation room, our non-contact PPGi can still achieve an average accuracy of 96.62%.

INDEX TERMS Photoplethysmogram imaging (PPGi), non-contact surveillance, predictive adversarial adaptation, homographic filter, risk-sensitive generation, adaptive thresholding.

I. INTRODUCTION

Ubiquitous and unobtrusive measuring of human physiology has long been an immense hope in all fields and incubation rooms of obstetrics and gynecology (OB/GYN). Unobtrusive

The associate editor coordinating the review of this manuscript and approving it for publication was Mohammad Zia Ur Rahman.

This work is licensed under a Creative Commons Attribution-NonCommercial-NoDerivatives 4.0 License.
For more information, see https://creativecommons.org/licenses/by-nc-nd/4.0/

and reliable monitoring without wiring can be a euphoric alternative for newborns and parents. Photoplethysmography imaging (PPGi) is deemed an ideal alternative for continuous and non-contact surveillance of infant heart activities [1], [2]. However, PPGi has some challenges in the application of newborns. Because infants' skin is immature compared to adults, as shown in Fig. 1, the multi-layer reflection of light through babies' skin emits wide versatility of 'transformed colors' among individuals. The transformation from spectrum to visual color space is nonstandard and, therefore, renders the projected color unstable.

The unstable colors make skin classification problematic. Additionally, most pre-mature newborns are still in a weak condition, and their cardiovascular muscles can only change the hemoglobin density in a minute. Therefore, existing PPGi may not work properly, and a novel PPGi technology should be developed specifically for baby skins.

Several challenges in existing PPGi technologies remain, compared to their contact counterparts, photoplethysmography (PPG), albeit both are still far from clinically usable. First, PPG and PPGi are sensitive to disruptions, such as motion artifacts or skin deforms [3], [4]. Second, the retrieved pulse waveform is inaccurate due to the complex hemoglobin-light reflection relation in various wavelengths. Third, the reflection recorded from cameras strongly depends on the quality and properties of light sources, and the unexpected glares in the surface will saturate the photodetectors. For example, some pre-mature neonatal newborns are usually inside an incubator, which may cause difficulty sensing skin color changes [5]. Forth, the skin pixels in a picture frame cannot be identified, and therefore non-skin pixels hinder the correct identification of hemoglobin density changes. Fifth, newborns usually are covered by minute hairs, which may interfere with the color detection and extraction algorithms. Last, the current laws follow stringent regulations to protect the vulnerable from any experiments. Therefore, few studies are explicitly made for newborns, e.g., [6] and [7].

Most PPGi algorithms try to avoid the above-mentioned problems by taking a spatial or temporal average of a roughly identified area in the frame-wise video image sequence. If the disturbances are minor, the averaging will only decrease the accuracy of the pulsation waveform. If the influence happens to be reversed with the pulses, the disturbances may cause the pulsatile components to disappear. However, the actions to counteract the various influences may contradict each other. For example, a large region of interest (ROI) is often taken to mitigate the edge problem of motion, but it manifests the inhomogeneity problem for a significant skin. Tracking multiple ROI nevertheless increases the burden of real-time computation. Because our goal in this paper is to develop an algorithm to keep tracking the smallest regions of baby skins with homogenous pulsation properties, our ROI may not be a contingent region, and, instead, it could be discrete pixels after excluding some inhomogeneous pixels. Therefore, the popular neural network methods for machine vision are unsuitable for pixel-oriented operation.

In this study, we tackle the above-mentioned challenges with a reliable skin pixel conditioning method with an adaptive generative tracking process. Based on the extracted pulsation, we synthesize the corresponding pulsation signals on the flight to identify the living portion in a scene with a spatiotemporal image sequence. The classifier dynamically determines suitable intervals or thresholds to identify the true skin pixels for effectively extracting PPGi. We capture those pixels with periodic variations and maximize the coherence of the extraction algorithm. The periodic variations are matched by a synthesized pulse from the output PPG signals through the control of a risk-sensitive filter.

II. METHODS

To monitor newborn heart activity through the skin surface, we must overcome the challenge of color variations in newborns' skins and the restricted lighting condition in incubation rooms. We develop a sufficiently robust algorithm to detect the pulse change from accurately identified skins (Fig. 2). The significant difference from other studies is the frequency tracking mechanism. We don't estimate heart rate directly. Instead, we synthesize and synchronize a frequency-controlled wave to the extracted wave from the skin ROI by estimating the frequency of a frequency synthesizer. In summary, filters in the algorithm are used for two different purposes. The risk-sensitive filter estimates parameters, while the Kalman filter rejects noises.

Approval of all ethical and experimental procedures and protocols was granted by the Institutional Review Board of Kaohsiung Medical University Hospital (KMUH) under Approval No. KMUHIRB-SV(I)-20210007.

A. PREDICTIVE ADVERSARIAL ADAPTATION

Swiftly distinguishing the skins and non-skins is key in the first step of providing high-quality ROI. As shown in Fig. 3, the pulse maximizer synthesizes a pulse according to a segment of past pulses by minimizing the synthesizing error. The ROI classifier seeks a valid threshold range to distinguish skin/non-skin regions by maximizing the extraction coherence. We use a color-based method in an iteration with max-min equilibrium to effectively separate luminance interference from the wide range of skin color.

As shown in Fig. 4, the pulse maximizer component in Fig. 3 operates in two phases. The process learns the illumination model in a calibration phase, while the synthesized pulses are generated by tuning the synchronizer in an online tracking phase. Training is performed on the specific calibration phase for the fixed part of the pulse maximizer. The trained model is then used for the online tracking phase. The predicted pulse will be generated and synchronized with the extracted waveforms in the PPG extractor. Simultaneously maximizing and minimizing the objectives resembles the principle of generative methods in recent prominent research [8]. The random-effect decoupler is trained to separate the influence of illumination. Let the training set $Z(s)$ and $Y(s)$ be the pixel values with and without the influence of illumination, respectively. $Z(s)$ and $Y(s)$ are vectors in a color space

(a) reddish skin (b) dark and hairy skin (c) normal skin (d) reddish and shaky

FIGURE 1. Samples of the wide range of newborns' skins. Our method of photoplethysmography imaging is suitable for such versatile skins.

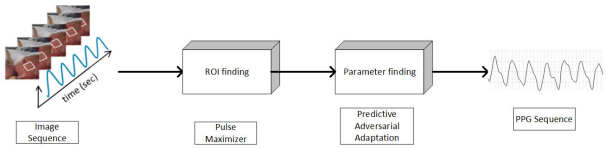

FIGURE 2. The flowchart of our algorithm. The significant skin straits are identified from input images. The next step is to dynamically adjust the parameters to keep the pulses clear.

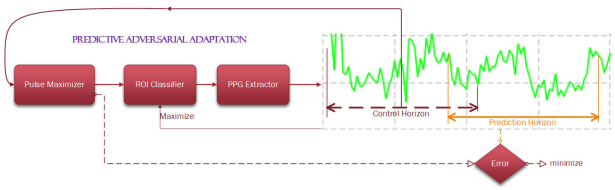

FIGURE 3. The iteration of the adaptive process comprises a pulse maximizer and ROI classifier before sending to pulse extraction. The pulse maximizer synthesizes a pulse according to a segment of past pulses by minimizing the synthesizing error. The ROI classifier seeks a valid threshold range to distinguish skin/non-skin regions by maximizing the extraction coherence. A color-based method is used in an iteration with max-min equilibrium; therefore, luminance interference can be effectively separated from the wide range of skin color.

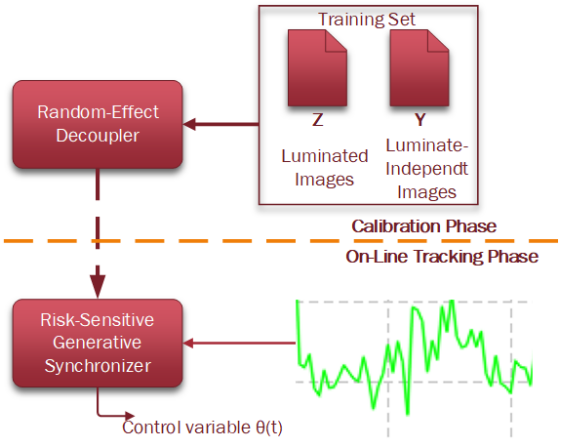

FIGURE 4. The pulse maximizer component in the Fig. 3 has two phases: supervised learning is performed in the random-effect decoupler at the calibration phase, and a pulse is synthesized in the risk-sensitive generative synchronizer at the online tracking phase. The control variable $\theta(t)$ is defined as in (6).

$\mathcal{C} = \{\mathcal{C}_1, \mathcal{C}_2, \mathcal{C}_3\}$, i.e., $Y(s) = \{y_i(s)\}_{i=\mathcal{C}_1,\mathcal{C}_2,\mathcal{C}_3}$ at a spatial point $s \in [1, \cdots, n] \times [1, \cdots, m]$ for an image with size $n \times m$. Denote all pixels in an image as matrices $\mathbf{Z} = \{Z(s)\}_{\forall s}$ and $\mathbf{Y} = \{Y(s)\}_{\forall s}$. We model the camera illumination process as an illumination-reflectance model under a distribution of illumination $\mathbf{F} = \{F(s)\}_{\forall s}$. The influence of $\mathbf{F}$ to $\mathbf{Y}$ is multiplicative through an influence matrix M_C under the transformation rule of the color space of $\mathbf{Y}$, that is, the resulting pixels become $\mathbf{F}\,M_C\,\mathbf{Y}$. For simplicity, we write the resulting influence $\mathbf{F}_C\mathbf{Y} \triangleq \mathbf{F}\,M_C\,\mathbf{Y}$ as a short notation.

$$\mathbf{Z} = \mathbf{F}_C\mathbf{Y} + \mathbf{v} + \boldsymbol{\xi}, \tag{1}$$

where $\mathbf{v}$ and $\boldsymbol{\xi}$ represent a small-scale spatially correlated random effect and a fine-scale uncorrected random noise, respectively. The uncorrected random noise is easy to be understood. The correlated random effect refers to the covariance arising from the diffusive process of lights and connected regions in an image. Assuming that random effects are of zero means, we can decompose the correlated zero-mean random process $v(s) = \sum_{s' \in [1,\cdots,n]\times[1,\cdots,m]} \phi(s', s)\psi(s')$, where $\phi(s', s)$ is the kernel density functions and $\psi(s')$ is the coefficient vector. The collected pixels in an image can be written in matrix form $\mathbf{v} = \Phi\Psi$, where $\mathbf{v} = \{v(s)\}_{\forall s}$, $\Phi = \{\Phi(s)\}_{\forall s}$, and $\Psi = \{\Psi(s)\}_{\forall s}$.

A homographic filter is a filter in the form [9], [10]

$$\mathcal{H} = \mathcal{H}(s; \gamma_L, \gamma_H) = (\gamma_H - \gamma_L)\left[1 - e^{-D^2(s)/2D_0^2}\right] + \gamma_L, \tag{2}$$

where $D(s)$ is the magnitude part of the point s in the Fourier plane, i.e., the distance from s to the origin, D_0 is a cutoff radius excluding the region near the origin, the parameters γ_L, γ_H satisfy $\gamma_H > \gamma_L \geq 0$. Rewrite (1) to

$$\ln[\mathbf{Z} - \mathbf{v} - \boldsymbol{\xi}] = \ln[\mathbf{F}_C\mathbf{Y}], \tag{3}$$

apply the filter with convolution $\circledast$. Set an operator $\mathcal{H}_{(u)} = e^{\mathcal{H}} \circledast \ln(u)$ for any image u. For example $\mathcal{H}_{F_C} = e^{\mathcal{H}} \circledast \ln(\mathbf{F}_C)$, $\mathcal{H}_{Z-v} = e^{\mathcal{H}} \circledast \ln(\mathbf{Z} - \mathbf{v})$, and $\mathcal{H}_Y = e^{\mathcal{H}} \circledast \ln(\mathbf{Y})$.

We can then find the parameters $\{\gamma_i\}_{i=\{L,H\}}$ in $\mathcal{H}$ such that $\mathcal{H}_{F_C} \approx \mathbf{I}$, the identity. Therefore, taking expectation to (3), we, therefore, obtain the decoupled pixels (4) for the next generative step.

$$\mathrm{E}[\mathcal{H}_{Z-v}] = \mathrm{E}[\mathbf{I}\mathcal{H}_Y], \tag{4}$$

where the expectation E is taken on the noise terms of the pixels, and therefore the Gaussian noise $\boldsymbol{\xi}$ is depressed.

The learners are trained to fit the coefficient matrix Ψ and the filter parameters (γ_i), based on a sequence of calibration records $(\mathbf{Z}, \mathbf{Y})$ in training and testing of the model (4), as shown in Fig. 4. The goal of the first phase learners is to reduce the influence of the wide variety of illumination sources to a steady one. Therefore, the identification performs both on filter parameters and the kernel coefficients of random effects. The singularity problem is often resolved during the computation through a regularization method with a Lagrange multiplier.

We are further generalized the regularized optimization problem in l_1 space [11] to avoid over-fitting. Therefore, the solution to the multivariate optimization problem becomes

$$\max_{\lambda} \min_{\Psi(s),\gamma_i} \|\mathcal{H}_{Z-v} - \mathcal{H}_Y\|_2^2 + \lambda \left\{(1-\sigma)/2\|\Psi\|_2^2 + \sigma\|\Psi\|_1\right\}. \tag{5}$$

where λ is the Lagrange multiplier of the constraint and σ is the penalty coefficient between l_1 and l_2, which define the norms $\|\cdot\|_1$ and $\|\cdot\|_2$, respectively. The optimization (5) is regulated by the Lasso (Least Absolute Shrinkage and Selection Operator) penalty when $\sigma = 1$ or the ridge penalty when $\sigma = 0$. Due to the properties of the l_1 space, the optimization (5) tends to find solutions with minimal non-zero elements, and it will yield strong reconstruction performance if several sparsity properties, such as restricted isometry and incoherence properties, are satisfied [12]. In our multivariate transformation matrix Ψ, the Lasso penalty tends to reduce the coefficients of less important covariates to zero, thus generating more zero solutions and satisfying the common requirement of black backgrounds. The ridge penalty compensates for the problem of multicollinearity by finding a balance between variance and bias [13], and effectively reducing the variance of identified coefficients [14], [15]. In summary, the parameters estimated in the first phase model (5) are $\{\gamma_L, \gamma_H, \Psi(s)\}$.

B. RISK-SENSITIVE GENERATIVE SYNCHRONIZER AND PULSE EXTRACTION

We must have an improved pulses extraction algorithm to adapt to infants' weak and fast heartbeats. Based on infants' skin properties, a specialized algorithm is developed for pinpointing a reliable ROI in the ROI classifier (Fig. 3). To further distinguish skin from non-skin, we assume those pixels varying with PPGi signals are skins, and non-periodic pixels are non-skins. In the tracking phase, we generate an artificial pulse $\tilde{p}(t;\theta)$, which is synchronized with the extracted signal $p(t)$, according to a regulated parameter

$$\theta(t) = \alpha(t)\mathrm{E}_{s\in Tw}[p(s)] + (1-\alpha(t))\theta(t-1), \tag{6}$$

where $Tw = [t_1, t_2]$ and $t_2 < t$ is a period of past time for control (the control horizon in Fig. 3 and $\alpha(t)$ is a decision variable that controls the proportion to depend on the history. We set $\tilde{p}(t;\theta) = \sin(\omega_0\theta t)$ with a scaling constant ω_0. The decision $\alpha(t)$ will be optimized to minimize the error $|p(t) - \tilde{p}(t;\theta)|^2$.

To accommodate uncertainty, we apply a risk-sensitive filter, which is an improved version of the Kalman filter [16]. To slightly sacrifice optimality, we replace the cost function with the risk-sensitive one and obtain good performance in the dynamic tracking of the generative process. The risk-sensitive filtering is given as

$$\alpha(t) = \arg\min_{\alpha(t)} \left\{J = \mathrm{E}[e^{(\beta\Phi_{0,t})}]\right\}, \ \beta > 0, \tag{7}$$

$$\Phi_{0,t} = \Phi_{0,t-1} + \frac{1}{2}(p(t) - \tilde{p}(t;\theta))Q(p(t) - \tilde{p}(t;\theta))^T, \tag{8}$$

where J is the cost functions taking expectation with weighting matrix Q, $\beta > 0$ is a risk-sensitive parameter for the extent of risk aversion. The recursive estimator from time t_1 to t_2 takes the form $\Phi_{t_1,t_2} = \frac{1}{2}\sum_{t=t_1}^{t_2}(p(t) - \tilde{p}(t;\theta))Q(p(t) - \tilde{p}(t;\theta))^T$. For example, the initial estimator takes range from 0 to t but (8) backward evaluates to the range $[0, t-1]$, which matches the range with $t_1 = 0$ and $t_2 = t-1$. Therefore, the range keeps shrinking until reaching the identity $\Phi_{0,0} = \mathbf{I}$.

Risk-sensitive filters aim to minimize variance estimation to obtain the best estimation while considering tolerance in modeling correctness. In contrast, risk-sensitive filtering can absorb the errors in the generative process. Therefore, measurement error and unidentified noise will not make the convergence process unstable.

In [17], the Cb-Cr intervals or thresholds for skin/non-skin discrimination are pre-defined such that $\gamma_{Cb_L} \le \mathrm{Cb} \le \gamma_{Cb_H}$ and $\gamma_{Cr_L} \le \mathrm{Cr} \le \gamma_{Cr_H}$. Differing from such fixed ROI classifiers, we dynamically adjust the classification intervals $[\gamma_{Cb_L}, \gamma_{Cb_H}]$ and $[\gamma_{Cr_L}, \gamma_{Cr_H}]$ to maximize the next step performance such that

$$\max_{\gamma_{Cb_L},\gamma_{Cb_H},\gamma_{Cr_L},\gamma_{Cr_H}} G_{pp}, \tag{9}$$

where G_{pp} is the auto-spectral density of the extracted PPGi signal $p(t)$. The result of the ROI classifier is a set $\mathcal{R}$ containing those pixels falling into the classification intervals. The ROI pixels also perform a histogram normalization step for the skin/non-skin segmentation and produce the index set $\mathcal{R}$ to mark the skin pixels.

In the next step, in the standard RGB color space $\mathcal{C} = \{R, G, B\}$ and an identified ROI with index set $\mathcal{R}$, the luminance decoupled pixels at time t are denoted that $Y_{\mathcal{R}}(t) = \{Y(s,t) | s \in \mathcal{R}, \text{at time } t\}$, where $Y(s,t)$ is the pixel at location s and time t. Notice that $Y_{\mathcal{R}}(t)$ takes values at $\mathbb{R}^3$ in 3 color channels. Instead of considering all wavelengths of incident lights, we adopt a notion of the 3-color channels,

(a) environment (b) incubator

FIGURE 5. (a) The camera and environment setup. (b) A baby slept inside an incubator.

which reflects the convolution responses of optical sensors of a camera in three ranges of wavelengths. After performing the principal component analysis (PCA), two principal components are obtained from the transformation of the matrix $Y_{\mathcal{R}}(t)$. The pulse $p(t)$ is extracted from the two values. Please refer the XminusαY algorithm [18].

Finally, a small fraction of spare time before the arrival of the succeeding picture frame can be used for noise filtering. We apply a Kalman filter to rectify the random fluctuation and a high-pass filter to remove the trend. Because some informative details of PPGi are mixed with broadband noises, we must not sacrifice too much of the high-frequency components while filtering the signals. Therefore, the two filters are controlled under a limited influence. We do not need to perform this step if all the precedent steps are sufficiently reliable. This step should alter the waveform as minor as possible.

The signal $p(t)$ sends to a Kalman filter with filter coefficient matrices T, C, D, G such that

$$\begin{aligned} \dot{\hat{p}}(t) &= T\hat{p}(t) + Dw(t), \\ p(t) &= C\hat{p}(t) + Gv(t), \end{aligned} \tag{10}$$

where $p(t)$ is the observed PPGi signal, $\hat{p}(t)$ is the true signal without artifacts and noises, $w(t)$, $v(t)$ are the Gaussian noises, respectively.

III. ANALYSIS

As shown in Fig. 5, we set up an observation environment in an incubation room. The incubator glass or plastics may cause some difficulty sensing the blood volume changes on the skin surface. However, our generative process can still overcome the challenge and get the expected result.

We obtain the pulse signals by applying the algorithms in the Section of Methods, and the results have been cross-validated against standard medical instruments. The experiment videos are taken from a 1080p HD camera in 60 frames per second. Our algorithm does not require high computation power; the real-time requirement is attained in an ordinary laptop computer (MS Surface Pro). As shown in Fig. 1, the collected babies' skin colors offer much versatility among individuals. Therefore, this section shows that our method accommodates such variation.

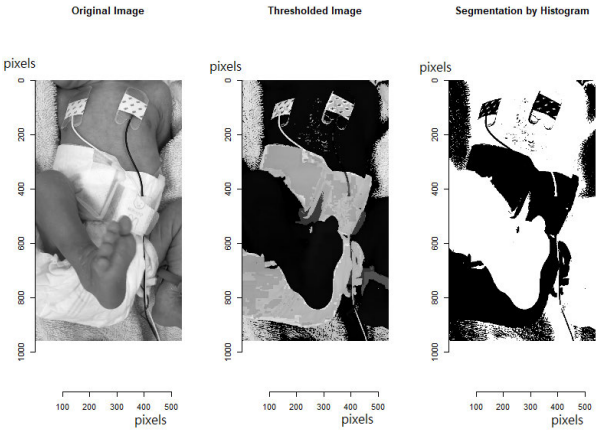

FIGURE 6. The classification results of our predictive adversarial adaptation for a baby wearing a diaper. (The video size was 540 × 960.) From Left to Right: a normal picture, the pulse maximizer output, the ROI classifier output.

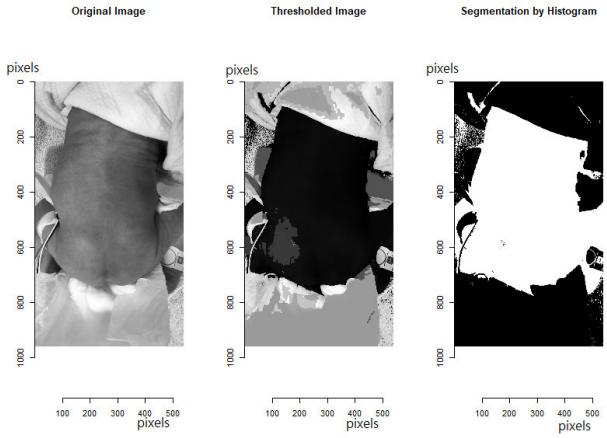

FIGURE 7. The classification results when an infant's skin is reddish. The color pictures are shown in Fig. 1. (The video size was 540 × 960.) From Left to Right: a normal picture, the pulse maximizer output, the ROI classifier output.

A. QUALITY OF PPGi APPLIED TO INFANTS

The output of the pulse maximizer precisely finds all the skin pixels. Our classification finds high-quality ROIs, as shown in Figs. 6-8. In Fig. 6, we can accurately identify the skin pixels for a high-quality classification, even for a baby wearing a diaper.

In Fig. 7, when the color appearance is far from the colors of ordinary skins, the random-effect decoupler in the pulse maximizer still can learn the model and separate the skin pixels for the consequent processes. Even though a blanket covers most skins, the ROI classifier still can produce high-quality ROI through Eq. (9) and the histogram normalization step (Fig. 8).

Fig. 9 compared the results side by side. The left half graphs were our results, and the right half graphs were obtained from an oximeter. We can see the instantaneous heart rate of both sides agreeing with each other.

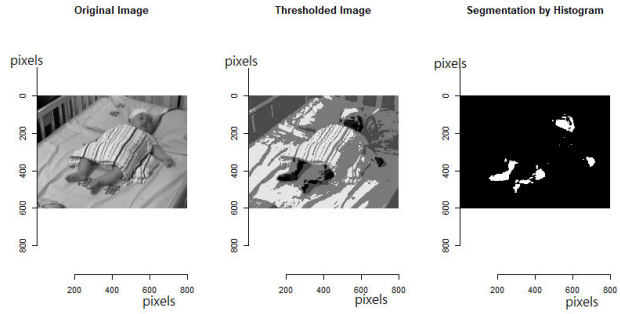

FIGURE 8. The classification results if a blanket covered most skins. Only 12% of pixels in the picture only appear to be skin. The ROI classifier can still produce high-quality ROI through Eq. (9) and the histogram normalization step. (The video size was 800 × 600.) From Left to Right: a normal picture, the pulse maximizer output, the ROI classifier output.

TABLE 1. Heart rate estimation of five infants in a 5-minute extraction.

case #	skin/picture ratio	activity	ECG bpm	estimated bpm	error
1	41%	quiet	100	103	2.9%
2	12%	sleeping	113	116	2.6%
3	11%	crying	173	167	3.6%
4	7%	sleeping	116	112	3.6%
5	6%	crying	138	144	4.2%

We also connected the subjects to a standard oximeter and cross-verified our results.

In Table 1, the error rate increases when the skin ratio becomes small, and the body moves swiftly. From the perfect to the most challenging situation, the errors increase from 2.9% to 4.2%. The average error rate was 3.38% or 96.62% in terms of accuracy. Our ROI aims to find those pixels that follow the same heartbeat trend. Because our ROI algorithm does not perform face identification nor keep contingent region, the pixelized ROI can completely utilize every pixel in the group average. Therefore, the consequent extraction can have superior accuracy.

B. RELATION TO RELATED RESEARCH

In the healthcare and transportation industry, contact-based PPG is applied to vital sign monitoring for hospitalized, home health care, rehabilitation, elderly nursing patients, and drivers [19], [20]. In professional sports training, such simple PPG devices are apt to record history in the field and perform optimization for training [21], [22].

This study tries to remedy three streams of research gaps. Compared to the contact-based methods, the non-contact ones are more attractive in infant monitoring domains, but they are generally considered weak in acquiring the exact details of cardiac information [3], [23] The golden standards in diagnosis are often based on the evidence of ECG [24], [25]. At the same time, contact-based and non-contact-based methods suffer from the same disadvantages in optical modeling. For example, the uneven contact force on the skin surface makes the photoplethysmographic signals irregular [26]. Wireless transmission of ECG signal still needs trained professionals to prepare contact surfaces [27].

Therefore, due to broad application domains, the earnings from PPGi exceed the investment to resolve image-related issues. Furthermore, recent advancement demonstrates that accurate measurement of specific physiological parameters becomes promising, and limitations on non-contact PPG are resolved gradually. Excellent publications offer systematic introductions for this line of technologies [4]. Most physiological studies still concentrate on heart rate counting on facial video [28]. Other applications slowly emerge, for example, a preliminary indicator of blood pressure [29]. We can see that the distances between subjects and cameras can be far, environmental disturbances become resistive, and movement artifacts become irrelevant.

For situations requiring long-term monitoring, such as neonatal intensive care unit (NICU), using camera photoplethysmography is ideal for infants [30]. Many studies suggest PPGi is suitable for continuously monitoring heart rate in neonatal intensive care unit [31], [32]. The advantage of non-contact sensing makes the PPGi suitable for applying to NICU [33], [34]. A complete system with comprehensive audio and video capacity in the NICU is remarkably suggested [35]. However, the skin surface of infants possesses special properties, and the standard techniques of image processing usually prevent the correct retrieval of skin pixels [32], [36].

Natal monitoring has different challenges compared to adult environments. Color distortion in a time-varying fashion and multi-layer reflection becomes a problem in the baby monitor. Because babies' skin is much thinner than adults, the light can easily penetrate subcutaneous tissue with rich hemoglobin and other particles. Therefore, without retrieving the light spectrum and estimating the reflectance, the reflected color will always keep changing. A quick solution is to counteract the color distortion by color space mapping slightly [37], but it may not work persistently. Some studies stick the camera lens to a small area of the skin and make the skin fill the entire camera scene because newborns seldom move dramatically [38], [39]. However, it is unlikely to have nurses watch the pointing position of cameras all the time. Another method keeps tracking multiple ROIs to suppress the color distortion [31]. The tracking keeps extracting imaging features of small motion patches and projecting to a specific plane [40]. However, the method mainly resolves the color changes caused by motion, not by multi-layer reflection from babies' skin. Many studies resort to neural networks to bypass mathematical details [41]. Recent massive computations of neural networks also extend to the babies' situation [42], [43].However, without knowing the working mechanism, there is no way to make continuous improvements for the monitoring performance.

A viable skin-classifier algorithm must differentiate the hemoglobin reflection spectra similar to that of skin pigment because skin colors are versatile in different color spaces. Most segmentation methods are developed for a single image [44], but we need a method for a series of images or spatiotemporal image sequences. The additional temporal relation across moving objects can be an important feature in

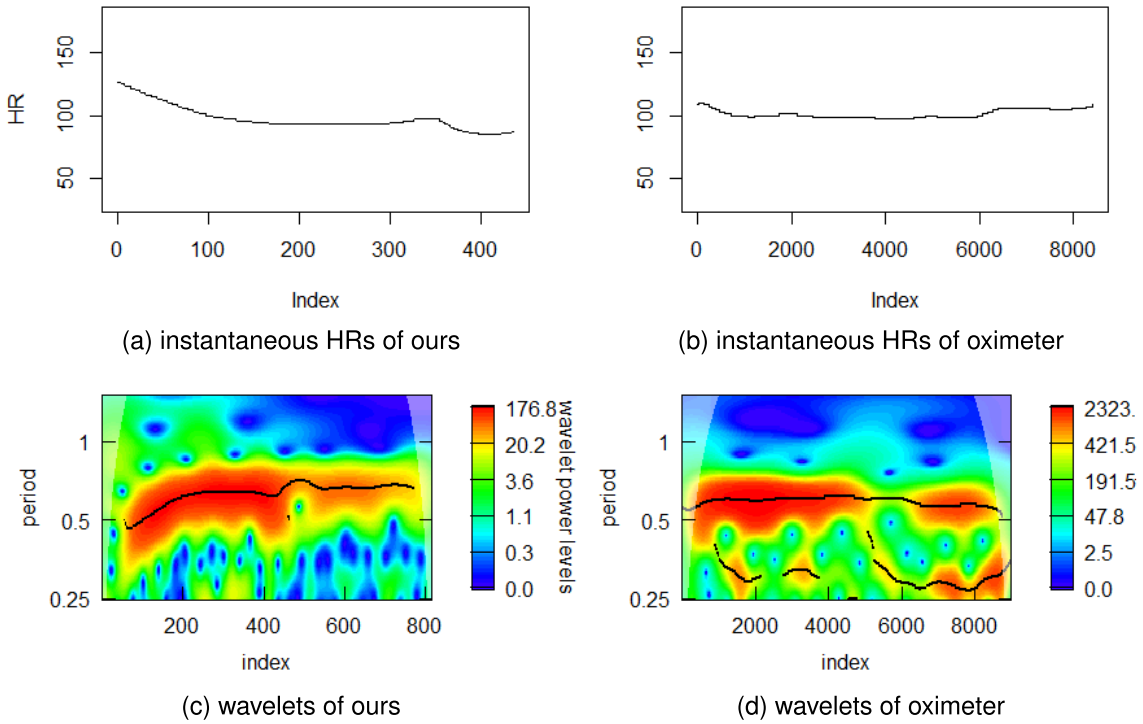

FIGURE 9. The upper two panels (a) (b) showed that the instantaneous heart rates (IHRs) were around 100 (case #1 in Table 1). The lower two panels (c)(d) showed the dominated ridges in the complex wavelet transform. The two left panels (a)(c) were the results calculated by our algorithm, and a medical oximeter measured the two right panels (b)(d). The resulting HRs agree with the readings of the oximeter.

segmentation [45]. More specifically, PPGi should perform skin detection on a video, not on every single picture.

Babies are unlike adults. To sense the hemoglobin reflection changes from an ordinary camera, the skin-classifier algorithms for newborns must accurately identify those pixels which are a part of the skin [36]. Demanding a baby's face toward the camera is difficult. Therefore, face detection algorithms may not work to extract the rich capillary on the face. On the other hand, as an online algorithm, timing constraints greatly limit the choice of feasible methods and the resulting accuracy.

Despite the challenges, the classifier does not need to identify all skin pixels. Only a few pixels are sufficient for consequent extraction. However, due to many inevitable factors, massively discarding suspicious pixels or performing spatial averaging still can not guarantee that the pixels are of skin or homogenous in reflection [45]. Nevertheless, the task of skin classification is only a small part of the entire extraction process, and we should not spend excessive time on this part.

Color-based skin detection methods are still the mainstream in time-sensitive applications [46]. Albert, the essential importance of the skin classifiers, a large number of similar studies and reviews keep popping out without pointing to a final perfect solution [47]. Regarding the wide variety of color spaces, skin and camera modeling, and illumination, each method has advantageous usages, and no single method can conquer other methods [48]. The threshold methods in HSV and YCbCr color space are quick and simple but of low quality [49]. A simple logic is used to separate skin pixels if the blue-difference (Cb) and red-difference (Cr) chroma components are within certain ranges because skins normally exhibit an elliptical color distribution [50]. For example, colors fall in the ranges, $77 \leq \text{Cb} \leq 127$ and $133 \leq \text{Cr} \leq 173$, can be deemed as skins [17]. However, the ranges may change as the conditions of races, ages, and illumination change. If the identified skin pixels contaminate with excessive non-skin pixels, the ordinary spatial averaging method will not recover the acquisition quality, and the consequent extraction algorithm will fail.

Empirical experiences demonstrate that color spaces should stick to cylindrical types (e.g., Hue-Saturation-Intensity), and lightness information should not discard due to the adaptation of color constancy algorithms to changing illuminance [51]. Among various color-based methods, instead of pre-determining a fixed threshold range to segment skins in a color space, dynamically adjusting such threshold range from the color histogram seems quick and of moderate quality.

Statistical-related methods in color-based skin detection could increase accuracy with a slight increase in processing time [47]. Additionally, theoretical game theory can help resolve the conflict for the skin classifier when the skin and non-skin strategies reach their Nash equilibrium [52]. A color clustering method, albeit it cannot increase quality but can adapt to a versatile environment for the skin classifier [53]. For region-based and shape-based methods, although contextual information or partial occlusion in faces, such as

wearing a face mask, can be detected, the speed and detecting quality are unsuitable for PPGi in general [54].

In the algorithms of skin detection, color distortion caused by motion represents a major obstacle in hindering the classifier's performance. An image's spatial redundancy can compensate for the distortion and construct a motion-robust PPGi [55]. A multi-objective optimization can also resolve the problem of skin inhomogeneity in heart rate estimation of PPGi [45]. Illumination changes in light sources are also key to the quality of PPGi. Specially designed multiple wavelength light sources are also reported to enhance the quality of photoplethysmographic imaging [56].

Among all the equally important steps of PPGi, extracting heart pulses on a reasonable skin reflection model has an overwhelming role in determining the final quality of PPGi signals. Blind source separation, a kind of principal component method, is a simple method to extract pulsated PPGi signal from regular RGB pixels [57]. A simplified skin model with chrominance cancellation in the reflection of skin pixels, CHROM, is one of the most popular pulse extraction methods [18]. The algorithm is then further reinforced by the signature of blood volume variation, which is called PBV, to compensate for the motion noise [58]. A plane-orthogonal-to-skin algorithm is also proposed for pulse extraction through dynamical principal components in synthesized color space [59], [60]. To make the extraction robust, skin features in wavelets on the hyperspectral information of skins are reported effective [61].

C. DISCUSSIONS

We additionally acquire PPGi of several newborns in the NICU and incubation room for cross-validation. Most of the babies are covered by blankets or clothes. For example, in the baby case #2, shown in Fig. 8 and in Table 1, related to the entire picture, the skins exposed outsize the blanket was counted as 12%, through the skin/nonskin discrimination in (9) with the maximized G_pp and the index set $\mathcal{R}$ for skin pixels. Although the skin part accounts for a small portion of the entire picture, we can still correctly identify the skins and accurately estimate bpm (beat per minute). We estimated that her heart rate was 116 bpm in a sleeping state, compared to the heart rate of 113 bpm measured by ECG.

For demonstration purposes, we listed a graphical sample of the experiments. In Fig. 9 (a) and (b), we can compare our results with the oximeter recorded manually from the life-supporting machine. The instantaneous heart rates (HRs) were obtained by taking a ridge analysis and producing the complex wavelet transforms in panels (c) and (d).

The heart rates shown in the graph are instantaneous heart rates, which reflect the frequency local to a time instance instead of counting the time for a heartbeat cycle. For example, ten complete cycles of heartbeats will produce ten numbers of heart rates during a period of 10 seconds but will produce an infinite number of instantaneous heart rates at any given instance of time without waiting for the 10 seconds.

Using instantaneous heart rate can effectively get accurate heart hearts and reject spurious spikes in the PPGi waveform. The resulting heart rates are congruent with the readings of the oximeter.

IV. CONCLUSION

In this study, we improve the PPGi quality for better use in non-contact PPGi by resolving existing challenges through a reliable skin classification algorithm with generated pulse trains. Based on the sensed pulsation, we synthesize the corresponding pulsation signals on the flight to identify the living skin in a spatiotemporal image sequence. We find that our two-phase adaptation method in risk-sensitive generative synchronizer effectively improves the quality of the resulting non-contact PPGi signal. Our algorithm produces substantial accuracy in the performance of PPGi reconstruction. In the limited illustration of the incubation room, our PPGi still has reliable results. This study contributes to cardiology by linking a low-cost, ubiquitous device to a conventional signal appearance. We bring low-cost acquisition to a usable level in incubation rooms.

Our algorithm produces substantial accuracy in the performance of non-contact PPGi reconstruction. In the limited illustration of the incubation room, our non-contact PPGi can still achieve an average accuracy of 96.62%, compared to the measure from ECG signals. According to the proposed non-contact usage scenario without wiring on a baby's skin, our algorithm and photographic devices can efficiently perform long-term surveillance in an incubation room without contact.

Recruiting volunteer parents to wire ECG electrodes on healthy infants is not easy. This study had limitations in experimental setup and the number of cases. We will keep pursuing and collecting more cases in healthy and NICU infants. Future development can improve robustness with different light sources, heterogeneous skin colors, and wide ranges of cardiovascular conditions.

ACKNOWLEDGMENT

(Yenming J. Chen and Lung-Chang Lin contributed equally to this work.)

REFERENCES

[1] S. Xu, A. Y. Rwei, B. Vwalika, M. P. Chisembele, J. S. A. Stringer, A. S. Ginsburg, and J. A. Rogers, "Wireless skin sensors for physiological monitoring of infants in low-income and middle-income countries," *Lancet Digit. Health*, vol. 3, no. 4, pp. e266–e273, Apr. 2021.

[2] C. B. Pereira, X. Yu, T. Goos, I. Reiss, T. Orlikowsky, K. Heimann, B. Venema, V. Blazek, S. Leonhardt, and D. Teichmann, "Noncontact monitoring of respiratory rate in newborn infants using thermal imaging," *IEEE Trans. Biomed. Eng.*, vol. 66, no. 4, pp. 1105–1114, Apr. 2019.

[3] A. M. Unakafov, "Pulse rate estimation using imaging photoplethysmography: Generic framework and comparison of methods on a publicly available dataset," *Biomed. Phys. Eng. Exp.*, vol. 4, no. 4, Apr. 2018, Art. no. 045001.

[4] A. V. Moco, "Towards photoplethysmographic imaging: Modeling, experiments and applications," Technische Universiteit Eindhoven, Eindhoven, The Netherlands, Tech. Rep., 2019.

[5] P. Simmen, S. Kreuzer, M. Thomet, L. Suter, B. Jesacher, P.-A. Tran, A. Haeberlin, S. Schulzke, K. Jost, and T. Niederhauser, "Multichannel esophageal heart rate monitoring of preterm infants," *IEEE Trans. Biomed. Eng.*, vol. 68, no. 6, pp. 1903–1912, Jun. 2021.

[6] Q. Chen, X. Jiang, X. Liu, C. Lu, L. Wang, and W. Chen, "Non-contact heart rate monitoring in neonatal intensive care unit using RGB camera," in *Proc. 42nd Annu. Int. Conf. IEEE Eng. Med. Biol. Soc. (EMBC)*, Jul. 2020, pp. 5822–5825.

[7] F. Voss, S. Lyra, D. Blase, S. Leonhardt, and M. Lüken, "A setup for camera-based detection of simulated pathological states using a neonatal phantom," *Sensors*, vol. 22, no. 3, p. 957, Jan. 2022.

[8] I. Goodfellow, J. Pouget-Abadie, M. Mirza, B. Xu, D. Warde-Farley, S. Ozair, A. Courville, and Y. Bengio, "Generative adversarial nets," in *Proc. Adv. Neural Inf. Process. Syst.*, 2014, pp. 2672–2680.

[9] C.-N. Fan and F.-Y. Zhang, "Homomorphic filtering based illumination normalization method for face recognition," *Pattern Recognit. Lett.*, vol. 32, no. 10, pp. 1468–1479, Jul. 2011.

[10] T. N. Le, D. B. Giap, J.-W. Wang, and C.-C. Wang, "Tensor-compensated color face recognition," *IEEE Trans. Inf. Forensics Security*, vol. 16, pp. 3339–3354, 2021.

[11] H. Zou and T. Hastie, "Regularization and variable selection via the elastic net," *J. Roy. Stat. Soc. B, Stat. Methodol.*, vol. 67, no. 2, pp. 301–320, Apr. 2005.

[12] E. J. Candès, "The restricted isometry property and its implications for compressed sensing," *Comp. Rendus Mathematique*, vol. 346, nos. 9–10, pp. 589–592, May 2008.

[13] D. W. Marquardt and R. D. Snee, "Ridge regression in practice," *Amer. Statistician*, vol. 29, no. 1, pp. 3–20, Feb. 1975.

[14] C. B. García, J. García, M. M. L. Martín, and R. Salmerón, "Collinearity: Revisiting the variance inflation factor in ridge regression," *J. Appl. Statist.*, vol. 42, no. 3, pp. 648–661, Mar. 2015.

[15] P. Exterkate, P. J. F. Groenen, C. Heij, and D. van Dijk, "Nonlinear forecasting with many predictors using kernel ridge regression," *Int. J. Forecasting*, vol. 32, no. 3, pp. 736–753, 2016.

[16] R. K. Boel, M. R. James, and I. R. Petersen, "Robustness and risk-sensitive filtering," *IEEE Trans. Autom. Control*, vol. 47, no. 3, pp. 451–461, Mar. 2002.

[17] F. Z. Chelali, N. Cherabit, and A. Djeradi, "Face recognition system using skin detection in RGB and YCbCr color space," in *Proc. 2nd World Symp. Web Appl. Netw. (WSWAN)*, Mar. 2015, pp. 1–7.

[18] G. de Haan and V. Jeanne, "Robust pulse rate from chrominance-based rPPG," *IEEE Trans. Biomed. Eng.*, vol. 60, no. 10, pp. 2878–2886, Oct. 2013.

[19] R. R. Singh, S. Conjeti, and R. Banerjee, "A comparative evaluation of neural network classifiers for stress level analysis of automotive drivers using physiological signals," *Biomed. Signal Process. Control*, vol. 8, no. 6, pp. 740–754, Nov. 2013.

[20] G. Fördős, I. Bosznai, L. Kovács, B. Benyó, and Z. Benyó, "Sensor-net for monitoring vital parameters of vehicle drivers," *ACTA polytechnica hungarica*, vol. 4, no. 4, pp. 25–36, 2007.

[21] M. Garbey, N. Sun, A. Merla, and I. Pavlidis, "Contact-free measurement of cardiac pulse based on the analysis of thermal imagery," *IEEE Trans. Biomed. Eng.*, vol. 54, no. 8, pp. 1418–1426, Aug. 2007.

[22] A. Mesleh, D. Skopin, S. Baglikov, and A. Quteishat, "Heart rate extraction from vowel speech signals," *J. Comput. Sci. Technol.*, vol. 27, no. 6, pp. 1243–1251, Nov. 2012.

[23] Q.-V. Tran, S.-F. Su, W. Sun, and M.-Q. Tran, "Adaptive pulsatile plane for robust noncontact heart rate monitoring," *IEEE Trans. Syst., Man, Cybern., Syst.*, vol. 51, no. 9, pp. 5587–5599, Sep. 2021.

[24] Y. Tao, Y. J. Chen, X. Fu, B. Jiang, and Y. Zhang, "Evolutionary ensemble learning algorithm to modeling of warfarin dose prediction for Chinese," *IEEE J. Biomed. Health Informat.*, vol. 23, no. 1, pp. 395–406, Jan. 2019.

[25] Y. Tao, Y. J. Chen, L. Xue, C. Xie, B. Jiang, and Y. Zhang, "An ensemble model with clustering assumption for warfarin dose prediction in Chinese patients," *IEEE J. Biomed. Health Informat.*, vol. 23, no. 6, pp. 2642–2654, Nov. 2019.

[26] X. F. Teng and Y. T. Zhang, "The effect of contacting force on photoplethysmographic signals," *Physiol. Meas.*, vol. 25, no. 5, pp. 1323–1335, Oct. 2004.

[27] C.-E. Tseng, J.-Y. Yen, M.-W. Chang, W.-C. Chang, and C.-K. Lee, "Modified frequency-partitioned spectrum estimation for a wireless health advanced monitoring bio-diagnosis system," *IEEE Trans. Syst., Man, Cybern. A, Syst. Humans*, vol. 40, no. 3, pp. 611–622, May 2010.

[28] M. A. Hassan, A. S. Malik, D. Fofi, N. Saad, B. Karasfi, Y. S. Ali, and F. Meriaudeau, "Heart rate estimation using facial video: A review," *Biomed. Signal Process. Control*, vol. 38, pp. 346–360, Sep. 2017.

[29] A. D. Choudhury, R. Banerjee, A. Sinha, and S. Kundu, "Estimating blood pressure using Windkessel model on photoplethysmogram," in *Proc. 36th Annu. Int. Conf. IEEE Eng. Med. Biol. Soc.*, Aug. 2014, pp. 4567–4570.

[30] M. E. Wieler, T. G. Murphy, M. Blecherman, H. Mehta, and G. J. Bender, "Infant heart-rate measurement and oxygen desaturation detection with a digital video camera using imaging photoplethysmography," *J. Perinatol.*, vol. 41, pp. 1725–1731, Mar. 2021.

[31] L. K. Mestha, S. Kyal, B. Xu, L. E. Lewis, and V. Kumar, "Towards continuous monitoring of pulse rate in neonatal intensive care unit with a webcam," in *Proc. 36th Annu. Int. Conf. IEEE Eng. Med. Biol. Soc.*, Aug. 2014, pp. 3817–3820.

[32] M. Villarroel, A. Guazzi, J. Jorge, S. Davis, P. Watkinson, G. Green, A. Shenvi, K. McCormick, and L. Tarassenko, "Continuous non-contact vital sign monitoring in neonatal intensive care unit," *Healthcare Technol. Lett.*, vol. 1, no. 3, pp. 87–91, Sep. 2014.

[33] M. A. Motin, C. K. Karmakar, and M. Palaniswami, "Ensemble empirical mode decomposition with principal component analysis: A novel approach for extracting respiratory rate and heart rate from photoplethysmographic signal," *IEEE J. Biomed. Health Informat.*, vol. 22, no. 3, pp. 766–774, May 2018.

[34] W. Wang, S. Leonhardt, L. Tarassenko, C. Shan, and D. McDuff, "Guest editorial: Camera-based monitoring for pervasive healthcare informatics," *IEEE J. Biomed. Health Informat.*, vol. 25, no. 5, pp. 1358–1360, May 2021.

[35] S. Cabon, F. Porée, G. Cuffel, O. Rosec, F. Geslin, P. Pladys, A. Simon, and G. Carrault, "Voxyvi: A system for long-term audio and video acquisitions in neonatal intensive care units," *Early Hum. Develop.*, vol. 153, Feb. 2021, Art. no. 105303.

[36] L. A. M. Aarts, V. Jeanne, J. P. Cleary, C. Lieber, J. S. Nelson, S. B. Oetomo, and W. Verkruysse, "Non-contact heart rate monitoring utilizing camera photoplethysmography in the neonatal intensive care unit—A pilot study," *Early Hum. Develop.*, vol. 89, no. 12, pp. 943–948, Dec. 2013.

[37] Q. Chen, Y. Wang, X. Liu, X. Long, B. Yin, C. Chen, and W. Chen, "Camera-based heart rate estimation for hospitalized newborns in the presence of motion artifacts," *Biomed. Eng. OnLine*, vol. 20, no. 1, pp. 1–16, Dec. 2021.

[38] M. R. Grubb, J. Carpenter, J. A. Crowe, J. Teoh, N. Marlow, C. Ward, C. Mann, D. Sharkey, and B. R. Hayes-Gill, "Forehead reflectance photoplethysmography to monitor heart rate: Preliminary results from neonatal patients," *Physiol. Meas.*, vol. 35, no. 5, pp. 881–893, May 2014.

[39] J. M. May, P. A. Kyriacou, and A. J. Petros, "Development of an optoelectronic sensor for the investigation of photoplethysmographic signals from the anterior fontanel of the newborn," in *Proc. Annu. Int. Conf. IEEE Eng. Med. Biol. Soc.*, Aug. 2011, pp. 18–21.

[40] Q.-V. Tran, S.-F. Su, and V.-T. Nguyen, "Pyramidal Lucas—Kanade-based noncontact breath motion detection," *IEEE Trans. Syst., Man, Cybern., Syst.*, vol. 50, no. 7, pp. 2659–2670, Jul. 2020.

[41] A. Akbari, J. Martinez, and R. Jafari, "A meta-learning approach for fast personalization of modality translation models in wearable physiological sensing," *IEEE J. Biomed. Health Informat.*, vol. 26, no. 4, pp. 1516–1527, Apr. 2022.

[42] F.-T.-Z. Khanam, A. G. Perera, A. Al-Naji, K. Gibson, and J. Chahl, "Non-contact automatic vital signs monitoring of infants in a neonatal intensive care unit based on neural networks," *J. Imag.*, vol. 7, no. 8, p. 122, Jul. 2021.

[43] Á. Nagy, P. Földesy, I. Jánoki, D. Terbe, M. Siket, M. Szabó, J. Varga, and Á. Zarándy, "Continuous camera-based premature-infant monitoring algorithms for NICU," *Appl. Sci.*, vol. 11, no. 16, p. 7215, Aug. 2021.

[44] A. Lumini and L. Nanni, "Fair comparison of skin detection approaches on publicly available datasets," *Expert Syst. Appl.*, vol. 160, Dec. 2020, Art. no. 113677.

[45] R. Macwan, Y. Benezeth, and A. Mansouri, "Heart rate estimation using remote photoplethysmography with multi-objective optimization," *Biomed. Signal Process. Control*, vol. 49, pp. 24–33, Mar. 2019.

[46] S. Naji, H. A. Jalab, and S. A. Kareem, "A survey on skin detection in colored images," *Artif. Intell. Rev.*, vol. 52, no. 2, pp. 1041–1087, Aug. 2019.

[47] M. A. Chyad, H. A. Alsattar, B. B. Zaidan, A. A. Zaidan, and G. A. A. Shafeey, "The landscape of research on skin detectors: Coherent taxonomy, open challenges, motivations, recommendations and statistical analysis, future directions," *IEEE Access*, vol. 7, pp. 106536–106575, 2019.

[48] K. B. Shaik, P. Ganesan, V. Kalist, B. S. Sathish, and J. M. M. Jenitha, "Comparative study of skin color detection and segmentation in HSV and YCbCr color space," *Proc. Comput. Sci.*, vol. 57, pp. 41–48, Jan. 2015.
[49] J. A. M. Basilio, G. A. Torres, G. S. Pérez, L. K. T. Medina, and H. M. P. Meana, "Explicit image detection using YCbCr space color model as skin detection," *Appl. Math. Comput. Eng.*, pp. 123–128, Jan. 2011.
[50] A. Kaur and B. V. Kranthi, "Comparison between YCbCr color space and CIELab color space for skin color segmentation," *Int. J. Appl. Inf. Syst.*, vol. 3, no. 4, pp. 30–33, 2012.
[51] R. Khan, A. Hanbury, J. Stöttinger, and A. Bais, "Color based skin classification," *Pattern Recognit. Lett.*, vol. 33, no. 2, pp. 157–163, 2012.
[52] D. Dahmani, M. Cheref, and S. Larabi, "Zero-sum game theory model for segmenting skin regions," *Image Vis. Comput.*, vol. 99, Jul. 2020, Art. no. 103925.
[53] S. Bobbia, R. Macwan, Y. Benezeth, A. Mansouri, and J. Dubois, "Unsupervised skin tissue segmentation for remote photoplethysmography," *Pattern Recognit. Lett.*, vol. 124, pp. 82–90, Jun. 2019.
[54] M. Sharma, S. Prakash, and P. Gupta, "An efficient partial occluded face recognition system," *Neurocomputing*, vol. 116, pp. 231–241, Sep. 2013.
[55] W. Wang, S. Stuijk, and G. de Haan, "Exploiting spatial redundancy of image sensor for motion robust rPPG," *IEEE Trans. Biomed. Eng.*, vol. 62, no. 2, pp. 415–425, Feb. 2015.
[56] J. Zheng, S. Hu, V. Azorin-Peris, A. Echiadis, V. Chouliaras, and R. Summers, "Remote simultaneous dual wavelength imaging photoplethysmography: A further step towards 3-D mapping of skin blood microcirculation," *Proc. SPIE*, vol. 6850, Feb. 2008, Art. no. 68500S.
[57] M.-Z. Poh, D. J. McDuff, and R. W. Picard, "Advancements in noncontact, multiparameter physiological measurements using a webcam," *IEEE Trans. Biomed. Eng.*, vol. 58, no. 1, pp. 7–11, Jan. 2011.
[58] G. de Haan and A. van Leest, "Improved motion robustness of remote-PPG by using the blood volume pulse signature," *Physiol. Meas.*, vol. 35, no. 9, pp. 1913–1926, Sep. 2014.
[59] W. Wang, S. Stuijk, and G. de Haan, "A novel algorithm for remote photoplethysmography: Spatial subspace rotation," *IEEE Trans. Biomed. Eng.*, vol. 63, no. 9, pp. 1974–1984, Sep. 2016.
[60] W. Wang, A. C. D. Brinker, S. Stuijk, and G. de Haan, "Algorithmic principles of remote PPG," *IEEE Trans. Biomed. Eng.*, vol. 64, no. 7, pp. 1479–1491, Jul. 2017.
[61] M. Denstedt, A. Bjorgan, M. Milanič, and L. L. Randeberg, "Wavelet based feature extraction and visualization in hyperspectral tissue characterization," *Biomed. Opt. Exp.*, vol. 5, no. 12, pp. 4260–4280, 2014.

YENMING J. CHEN received the Ph.D. degree in systems science and mathematics from Washington University in St. Louis, St. Louis, MO, USA, in 1998. He is currently a Distinguished Professor with the Department of Information Management, National Kaohsiung University of Science and Technology, Kaohsiung, Taiwan. He is the author of several books, patents, and more than 75 SCI/SSCI articles. His research interests include the IoT/AI, sound/spectrum technologies, fault detection, precision medicines, and medical computations.

LUNG-CHANG LIN received the bachelor's and Ph.D. degrees in medicine from Kaohsiung Medical University, Kaohsiung, Taiwan. He is currently the Director of the Department of Pediatric Neurology, Kaohsiung Medical University Hospital, Kaohsiung. He is also a Professor with Kaohsiung Medical University. His research interests include epilepsy, ADHD, and child development.

SHU-TING YANG received the M.D. degree from Kaohsiung Medical University, Kaohsiung, Taiwan, in 2000. She is currently a Attending Physician with the Division of Neonatology, Department of Pediatrics, Kaohsiung Medical University Hospital, Kaohsiung. Her current research interests include pediatrics and neonatology.

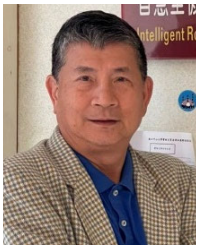

KAO-SHING HWANG (Member, IEEE) received the M.M.E. and Ph.D. degrees in electrical and computer engineering from Northwestern University, Evanston, IL, USA, in 1989 and 1993, respectively. He was with National Chung Cheng University, Taiwan, from 1993 to 2011, where he was the Deputy Director of the Computer Center, from 1998 to 1999; the Chairperson of the Department of Electrical Engineering, from 2003 to 2006; and the Director of the Institute of Opto-Mechatronics, from 2010 to 2011. He is currently a Distinguished Professor/A.S.E. Group Chair Professor with the Department of Electrical Engineering, National Sun Yat-sen University. He is also an Adjunct Chair Professor with Kaohsiung Medical University, Kaohsiung, Taiwan; a Distinguished Chair Professor with National Formosa University, Taiwan; and a Visiting Chair Professor with the Department of Computer Engineering, Northwestern Polytechnic University, Xi'an, China. His research interests include methodologies and analysis for various intelligent systems, visual servoing, and reinforcement learning for medical aid systems and robotic applications. He is a fellow of The Institution of Engineering and Technology (FIET). He received the MOST 2020 Outstanding Research Award, Taiwan.

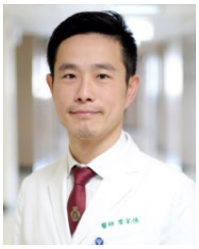

CHIA-TE LIAO holds the two M.Sc. degrees from the London School of Hygiene and Tropical Medicine, London School of Economics and Political Science, and the Doctor of Medicine degree from Taipei Medical University. He has been awarded dual Ph.D. degrees from National Cheng Kung University, Taiwan, and Leuven University, Belgium. Currently, he is a Cardiologist in Chi Mei Medical Center and an Assistant Professor at the National Sun Yat-sen University, Taiwan, Liao boasts an extensive publication record, with over 50 SCI articles and multiple books. His research areas encompass clinical trials, cardiological epidemiology, health economics, artificial intelligence in medicine, public health, and health policy.

WEN-HSIEN HO received the B.S. degree in marine engineering from National Taiwan Ocean University, Taiwan, in June 1991, the B.S. degree in industrial and information management from National Cheng-Kung University, in June 1998, and the M.S. degree in mechanical and automation engineering and the Ph.D. degree in engineering science and technology from the National Kaohsiung First University of Science and Technology, Taiwan, in June 2002 and January 2006, respectively. From September 1991 to July 2006, he was an Engineer with the Department of Design, CSBC Corporation, Taiwan. He is currently a Professor with the Department of Healthcare Administration and Medical Informatics, Kaohsiung Medical University, Taiwan. His research interests include intelligent systems and control, computational intelligence and methods, robust control, and quality engineering.